Newly designed metal foam-salt hydrate composite for thermochemical heat storage

Yutong Liu, Alexandre Dimanov, Didier Dalmazzone, Simon Hallais

Applied Energy

Newly designed metal foam-salt hydrate composite for thermochemical heat storage

--Manuscript Draft--

Manuscript Number:	
Article Type:	Research Paper
Keywords:	Thermochemical heat storage; Sorption; Selective water sorbent; Metal foam; Calcium chloride
Corresponding Author:	Yutong LIU Solid Mechanics Laboratory Palaiseau Cedex, FRANCE
First Author:	Yutong LIU
Order of Authors:	Yutong LIU
	Alexandre Dimanov
	Didier Dalmazzone
	Simon Hallais
Abstract:	Thermochemical heat storage system based on the sorption mechanism between water vapor and hygroscopic salts is considered to be a promising technology. However, hygroscopic salts have drawbacks such as swelling and agglomeration of the crystalline salt particles during hydration/dehydration cycles, which progressively leads to decreasing specific reaction surface and kinetics of heat and mass transfer, thus resulting in poor cyclic performance and stability. In this paper we propose a composite material, based on open-cell metal foam as host matrix, containing calcium chloride as hygroscopic salt dispersed in the pores. An open-cell metal foam host matrix improves the heat and mass transfer kinetics thanks to the porous structure and the high thermal conductivity, and offers additional advantages related to elevated mechanical strength, which would ensure mechanical resistance of the composite. The composite showed significant improvement in thermochemical performance compared to that of bulk calcium chloride powder in hydration/dehydration cycles. For cyclic stability, composites presented a slight increase and stabilization of thermal energy released upon cycles, while salt showed a substantial and continuous degradation of 78.5% in performance after 12 cycles. For heat released, composites outperformed considerably the bulk calcium chloride in almost all cycles. At the 12thcycle, the heat released of composites improved substantially to 5~6 times that of bulk calcium chloride powder. Observations by in situ environmental scanning electron microscope hydration/dehydration cycles demonstrate that swelling and deliquescence induce moderate redistribution of salt hydrates within the metal foam while preserving the essential open porosity of the matrix. It efficiently prevents extensive salt agglomeration and loss of specific reaction area, which explains the amelioration of the composite's thermochemical properties and cyclic stability. In conclusion, the metal foam-salt hydrate composite developed in our work is suitable and promising for thermochemical energy storage, offering both mechanical and thermochemical advantages.
Suggested Reviewers:	Christophe Coquelet christophe.coquelet@mines-albi.fr
	Henk Huinink h.p.huinink@tue.nl
	Jean-Pierre Bédécarrats jean-pierre.bedecarrats@univ-pau.fr
	Ruzhu Wang rzwang@sjtu.edu.cn

Declaration of interests

☒The authors declare that they have no known competing financial interests or personal relationships that could have appeared to influence the work reported in this paper.

☐The authors declare the following financial interests/personal relationships which may be considered as potential competing interests:

Newly designed metal foam-salt hydrate composite for thermochemical heat storage

Yutong Liu [a,*], Alexandre Dimanov [a], Didier Dalmazzone [b], Simon Hallais [a]

[a] LMS, UMR7649, Ecole Polytechnique, Institut Polytechnique de Paris, Route de Saclay, 91128 Palaiseau, France
[b] UCP/ENSTA Paris, Institut Polytechnique de Paris, Palaiseau, France
* Corresponding author. E-mail address: yutong.liu@polytechnique.edu

Note: Author names are in the form of "Given name + Family name".

Abstract

Thermochemical heat storage system based on the sorption mechanism between water vapor and hygroscopic salts is considered to be a promising technology. However, hygroscopic salts have drawbacks such as swelling and agglomeration of the crystalline salt particles during hydration/dehydration cycles, which progressively leads to decreasing specific reaction surface and kinetics of heat and mass transfer, thus resulting in poor cyclic performance and stability.

In this paper we propose a composite material, based on open-cell metal foam as host matrix, containing calcium chloride as hygroscopic salt dispersed in the pores. An open-cell metal foam host matrix improves the heat and mass transfer kinetics thanks to the porous structure and the high thermal conductivity, and offers additional advantages related to elevated mechanical strength, which would ensure mechanical resistance of the composite. The composite showed significant improvement in thermochemical performance compared to that of bulk calcium chloride powder in hydration/dehydration cycles. For cyclic stability, composites presented a slight increase and stabilization of thermal energy released upon cycles, while salt showed a substantial and continuous degradation of 78.5% in performance after 12 cycles. For heat released, composites outperformed considerably the bulk calcium chloride in almost all cycles. At the 12th cycle, the heat released of composites improved substantially to 5~6 times that of bulk calcium chloride powder. Observations by in situ environmental scanning electron microscope hydration/dehydration cycles demonstrate that swelling and deliquescence induce moderate redistribution of salt hydrates within the metal foam while preserving the essential open porosity of the matrix. It efficiently prevents extensive salt agglomeration and loss of specific reaction area, which explains the amelioration of the composite's thermochemical properties and cyclic stability. In conclusion, the metal foam-salt hydrate composite developed in our work is suitable and promising for thermochemical energy storage, offering both mechanical and thermochemical advantages.

Keywords

Thermochemical heat storage; Sorption; Selective water sorbent; Metal foam; Calcium chloride

1. Introduction

The global energy crisis has been exacerbated by a combination of factors such as the rapid economic rebound after the Covid-19 pandemic, extreme weather events, disrupted conventional energy supplies and geopolitical reasons, triggering an unprecedented momentum in the development of renewable energy. The soaring prices of conventional fossil energy sources have increased the competitive price benefit of renewable energy while raising awareness of the energy security advantages offered by domestically produced renewable energy worldwide. According to the International Energy Agency 2022 report on renewable energies, driven by existing and new policies introduced in China (the 14th Five-Year Plan), the European Union (the REPowerEU plan), the United States (the US Inflation Reduction Act), renewable energy capacity is expected to grow by 2400 GW, which accounts for more than 90% of global electricity capacity expansion over 2022-2027. It is anticipated that renewable energy overtakes coal as the world's largest source of electricity generation by early 2025 and its share of the electricity mix increases by 10% within five years to reach 38% in 2027 [1, 2].

Among all the renewable energies, the usage of solar energy is a current common trend worldwide for generating electricity via photovoltaics (PV) or by concentrating solar power (CSP) as well as for thermal applications related to space heating in domestic sectors [3, 4]. For both CSP plants and thermal applications such as heating buildings using solar energy, it is essential to be equipped with low-cost and reliable thermal energy storage (TES) system to cope with the mismatch between energy demand and supply, thereby compensating for the intermittent nature of renewable energy and providing energy on-demand [5]. There are mainly three existing TES technologies depending on the relevant physicochemical mechanisms, which are (1) sensible heat storage (SHS) [6, 7], (2) latent heat storage (LHS) [8, 9], and (3) thermochemical heat storage (THS) [10, 11]. SHS and LHS are considered as relatively mature technologies that have been developed and reached commercial implementation. Yet, thanks to their high energy density, small heat losses, flexibility for daily to seasonal heat storage, and significant cost reduction, the THS technology has attracted more attention and experienced prompt development in the past decades [7, 12-14].

Compared to storage mechanisms based on solely chemical reactions, THS systems based on sorption mechanisms have the advantage of low activation energies and are therefore suitable for low-temperature applications, such as domestic heating [3]. The sorption THS system can be applied either in open or closed systems [15]. For an open system, the reactant gas is directly provided from (or released to) the surrounding environment. Water vapor in the ambient air is the most convenient and cost-effective reactant gas. When compared to other open systems, the THS systems based on water vapor sorption/desorption are therefore the most simple, stable and environmentally friendly ones [16]. The open THS systems based on the reversible gas-solid reactions between thermochemical materials (TCM) and water vapor can be described as followed:

$$TCM \cdot nH_2O_{(s)} + \Delta H_r \rightleftharpoons TCM \cdot mH_2O_{(s)} + (n-m)H_2O_{(g)} \quad (1)$$

The optimal operation of TES depends to a large extent on the selection of a suitable TCM. An appropriate TCM should meet certain requirements, such as high energy storage density, elevated cycling stability, suitable operating temperature, stable mechanical properties, low or

non-toxicity and environmental neutrality, economic viability, and appropriate heat and mass transfer properties [3, 7, 17, 18]. As promising TCMs, pure hygroscopic salt hydrates and mixed salt hydrates have been widely studied in recent decades [19-24]. The ability of salt hydrates and water vapor systems to operate at a relatively low temperature suits well for applications such as seasonal and long-term energy storage. However, despite the generally high energy density offered by pure or mixed salt hydrates, problems related to high costs, restrictive operating conditions and the possible toxicity of certain salt prevent their large-scale deployment without special treatments [25-27]. Additionally, hygroscopic salts present non-negligible disadvantages such as excessive swelling and agglomeration during hydration/dehydration cycles, as well as potential deliquescence phenomenon if the relative humidity exceeds the deliquescence relative humidity (DRH), which progressively degrade heat and mass transfer efficiency and lead to poor cyclic stability [28-30].

To alleviate the limitations mentioned above and to make more efficient use of the high energy density of hygroscopic salts, a family of composite sorbents named selective water sorbents (SWS) or composite "salt in porous matrix (CSPM) has been proposed and designed by Aristov et al [31, 32]. The concept is to impregnate hygroscopic salts in a porous host matrix with open pores. This combined structure will limit excessive volume changes due to swelling and agglomeration by confining the salt crystals to the open pores, hence preventing loss of the reaction specific surface. In addition, the presence of pores also provides more efficient pathways for mass and heat transfer, which would both promote the kinetics of hydration/dehydration reaction [33]. The most commonly investigated composites concerned $CaCl_2$, LiCl, $MgSO_4$, $MgCl_2$, $SrBr_2$ salts, and host matrices with a pore size smaller than 50 nm, such as zeolites, silica gels, carbon-based materials, alumina, vermiculites and metal-organic frameworks (MOF) [34-43]. Despite the promising possibilities offered by these different composite systems to be applied to different applications under various operation conditions, these works still haven't been considered for commercial deployment because of problems related to inappropriate charging temperature, low thermal conductivity and possible leakage of the salt solution after deliquescence [28, 44, 45].

This paper presents an original CSPM type of SWS, specifically designed for thermochemical energy storage. The composite consists of open-cell metal foam with a pore size of about 350 μm as host matrix and calcium chloride as hygroscopic salt dispersed in the pores. Calcium chloride has been proposed as a promising TCM for decades, both as pure salt hydrate and as impregnated salt in composite form. It is an affordable industrial by-product offering many advantages such as high energy storage density, low cost, non-toxicity, and suitability for low-temperature operation conditions [46-51]. Open-cell metal foams are composed of interconnected pores that form a network in the structure [52]. A metal foam host matrix improves the heat and mass transfer kinetics thanks to the porous structure and the high thermal conductivity, and offers additional advantages related to elevated mechanical strength, which would ensure the mechanical resistance of the composite. What's more, the mechanical strength and relatively low density of metal foam serving as host matrix ensure the possibility of manufacturing lightweight and durable components, adapted to handling, stacking and mounting operations, which are necessary for adequate dimensioning and fabrication of flexible and polyvalent thermochemical reactors for future industrial and commercial TCM applications. Besides, the reticulation of large open porosity, with several hundred-micrometer pore sizes, provides large open volumes allowing for swelling of salt hydrates

without occluding pore spaces, and hence preserving the mass transfer kinetics. Therefore, metal foam–salt hydrate composites meet all requirements for the heat and mass transfer process which are essential for the good performances of thermochemical composites [53]. Additionally, metal foams can be produced using recycled metal materials, which offers additional environmental advantages [54].

This paper focuses first on the synthesis of appropriate metal foam-salt hydrate composite. Secondly, we evaluate their thermochemical properties during hydration/dehydration cycles and compare them with that of bulk salt hydrate powders. At last, the evolution of the thermochemical properties of composites is addressed based on their thermomechanical characteristics and in particular their microstructural/morphological evolution. For that purpose, we performed experimental measurements by differential scanning calorimetry (DSC) and in situ environmental scanning electron microscope (ESEM) observations.

2. Experimental methodology

2.1. Starting materials

Commercial nickel foam (Recemat BV) and aluminum foam (American Elements) with an average pore size of 350 μm were used as the host matrices of the composites (see Fig. 1). $CaCl_2 \cdot 2H_2O$ (VWR Chemicals, AnalaR NORMAPUR® Reag. Ph. Eur.) was used as the thermochemical active phase of the composite.

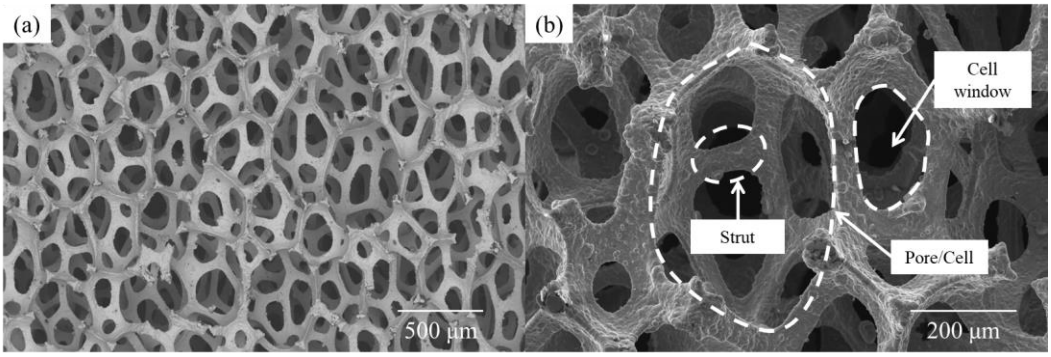

Fig. 1. (a) Backscattered Electron (BSE) image (x40 magnification) and (b) SEM image (x127 magnification) of commercial nickel foam used in this study for synthesizing the composite, with essential elements (pore/cell, strut, and cell window) of open-cell metal foam marked in dashed lines.

2.2. Synthesis of composite

The deposition of $CaCl_2$ particles into the metal foam matrix was realized by the deposition-precipitation process. The metal foams were cut into pieces in the form of panels, measured, and weighed before depositing $CaCl_2$. They were then immersed in an oversaturated solution of calcium chloride at room temperature. Dispersion of salt particles was achieved by stirring continuously and intensively the metal foam in the $CaCl_2$ solution for approximately 5 min. Then the composites were subjected to moderately flushed by compressed air to remove the excess salt dispersion from the pores and to avoid complete saturation of the porosity. The final step consisted of placing the composites in an oven for more than 48 h at 90 ℃.

2.3. DSC: thermal properties analysis

The thermal properties analysis of the composite was realized by performing thermal cycling tests on a DSC device (Micro-DSC VII, SETARAM). The DSC device was equipped with a

double chamber that serves as the calorimetric block. It contained one vessel for the sample and a second one for reference. Both vessels consisted of an 850 µl cylindrical crucible made of Hastelloy®. They were sealed with elastomer seals retained by anti-extrusion rings. The heat flow measurement sensor consisted of a high-sensitivity planar flow meter, which surrounded the two experimenting vessels and kept a tight thermal connection to the calorimetric block, ensuring identical temperature between the experimenting vessels and the calorimetric block. The temperature sensor was composed of Peltier elements with Joule effect calibration and provided measurement accuracy of a level up to ± 0.07 °C for the temperature range between -45 °C and 120 °C.

We performed cyclic thermal experiments on a nickel foam-$CaCl_2$ composite sample under vacuum conditions. The sample was heated up to 115 °C and cooled down to -40 °C at the heating/cooling rate of 0.5 °C/min for 4 cycles. The temperature range was chosen to cover the temperature range of possible working conditions for the composite serving as thermochemical material for thermal energy storage. To reduce the errors related to the thermal lag between the sample and the sensor, a relatively low heating and cooling rate of 0.5 °C/min was chosen [55]. The thermal properties of the composite were then analyzed based on the DSC curve recorded during the crystallization and melting process of the salt.

2.4. Calorimeter: thermal analysis during hydration/dehydration cycles

2.4.1. Experimental setup

Heat flow measurements during hydration and dehydration cycles were carried out on a Calvet-type calorimeter (C80, SETARAM). The sample and reference vessels of 12.5 ml were connected to a gas circulation tubing circuit. They were surrounded by 3D Calvet sensors based on thermocouples with Joule effect calibration which provided a temperature measurement accuracy of ± 0.1 °C and precision of ± 0.15 °C. The operating temperature range was between the ambient temperature and 300 °C.

The metal foam-salt composite samples were kept dry in the oven at 90 °C and re-weighed before use. Samples were then placed directly into the sample vessel of the calorimeter and sealed to prevent the hydration of the sample due to ambient air humidity. Every two samples of metal foam-salt composite panels were stacked in the sample vessel to simulate their practical industrial application conditions. For our experiment, we chose to perform the hydration/dehydration cycles at an isothermal condition at 23 °C. A bottle of dry nitrogen gas ($N_2 \geq 99.999\%$, ALPHAGAZ™ 1 Nitrogen, Air Liquide) was connected to two gas circuits controlled by a valve. During the dehydration process, the dry nitrogen gas served as the purge gas. For the hydration process, the dry nitrogen gas passed through a gas bubbler filled with a saturated solution of magnesium nitrate kept at a constant temperature of 23 °C by water bath, which allowed the nitrogen gas to be humidified to a constant relative humidity of 54% [56]. The nitrogen gas then passed a flowmeter (R-2-15-AA, Sho-Rate™ 1355, BROOKS) connected to the gas inlet tube of the sample vessel for measuring the gas flow rate. It can be controlled by adjusting the switch knob of the gas circulation tube attached to the sample vessel. For both the cyclic hydration and dehydration processes, the gas flow rate was controlled at 128 ml min^{-1}. Note that the inlet pipe connecting to the entrance of the sample vessel was heated by a water bath glass tube and was heat-insulated to ensure that the humidified gas could still enter the reaction chamber at the temperature of 23 °C so that the

fluctuations of heat flow in the reaction chamber due to temperature differences could be avoided. The gas outlet tube of the sample vessel was then linked to a vacuum pump to realize the gas circulation throughout the experimental setup. At the beginning and the end of each hydration/dehydration process, we waited for at least 15 min for the signal to stabilize. The schematic of the experimental setup is shown in Fig. 2.

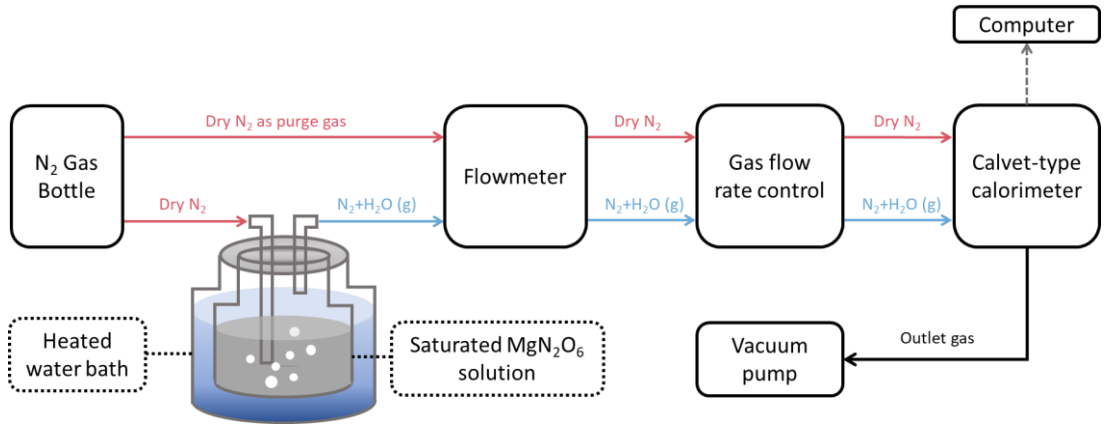

Fig. 2. Schematic diagram of the experimental setup.

2.4.2. Experimental procedures

For analyzing the thermal cycling performance of the composite and compare its performance with that of bulk $CaCl_2$ salt during hydration and dehydration cycles, we performed experiments on three kinds of samples, which were nickel foam-$CaCl_2$ composite (48.5 wt% $CaCl_2$), aluminum foam-$CaCl_2$ composite (21.0 wt% $CaCl_2$) and bulk $CaCl_2$ salt powder. We designed two kinds of experimental procedures described as follows.

1) Long hydration/dehydration cycles

To avoid the possibly irreversible structural damage of the composite related to leakage of $CaCl_2$ due to possible deliquescence during complete hydration, each composite sample was partially hydrated by the circulation of hydrated nitrogen gas with a constant relative humidity at 54% for different hydration duration Δt_{hydr} under isothermal conditions for 12 cycles (see Table 1). After every hydration, the samples were completely dehydrated by the circulation of dry nitrogen. The time necessary to completely dehydrate the sample depended on the hydration duration, the type of sample, and the mass content of salt in the composite. The same experimental procedure was applied to bulk salt powder for comparison.

Cycle number	Hydration duration Δt_{hydr} (min)
1	360
2	180
3	180
4	180
5	90
6	90
7	90
8	90
9	45
10	45
11	45
12	360

Table 1. Long hydration/dehydration cycles experimental procedure.

2) Short hydration/dehydration cycles

In this procedure, each sample was hydrated by the circulation of hydrated nitrogen gas with a constant relative humidity at 54% for 45 min under isothermal conditions and was completely dehydrated by the circulation of dry nitrogen after every hydration process. Six cycles of this experiment were performed for each kind of sample, and two repetition tests were conducted.

Heat flows during these cycles were recorded and the quantity of thermal energy released during each hydration/dehydration cycle was obtained by integrating the heat flow signal over the time duration of each experiment. Experimental errors were estimated according to the data acquired through repetition tests as well as resolution limitations of the instrument given by manufacturers.

2.5. SEM: in situ hydration/dehydration cycling test

In situ hydration/dehydration cycling tests of the metal foam-salt composites were performed using a scanning electron microscope (FEI QUANTA 650 FEG-ESEM) to investigate their microstructural evolution. The observation and the image recording in real-time during the process were done under controlled relative humidity (RH), which was made possible with the environmental scanning electron microscope (ESEM) mode and using a gaseous secondary electron detector (GSED) [57, 58]. In addition to RH control, the ESEM mode also allowed for avoiding coating the poorly conductive salt particles with conductive metal foam, hence preserving their original characteristics.

The nickel foam-$CaCl_2$ composite sample (7 mm × 7 mm × 1.4 mm) fresh out of the oven was mounted on a cooling stage using the Peltier effect with a thermocouple in contact with the sample's upper surface to monitor the actual temperature of the sample. For reproducing the experimental conditions of thermochemical tests mentioned in section 2.4, the sample was controlled at a constant temperature of 23 ℃ by adjusting the temperature of the Peltier stage. During the hydration process, the humidity around the sample was gradually increased from 0 to about 54% RH. This was achieved and controlled by increasing the vapor pressure in the scanning electron microscope (SEM) chamber. Likewise, for the dehydration process, the humidity was decreased to 0 by reducing the vapor pressure in the chamber. Highly resolved images (3072 × 2207 pixels per image with a pixel size of 0.08 μm) were taken for the region of interest (ROI) at the initial and final states for both hydration and dehydration cycles. Lower resolution images (1536 × 1113 pixels per image with a pixel size of 0.77 μm) were also recorded automatically every 5 seconds during the hydration/dehydration cycles.

3. Results and discussion

3.1. Thermal properties analysis of the composite

Thermal properties and thermal cyclic reliability of metal foam-salt composite were analyzed by DSC. Fig. 3 presents the DSC curves of nickel foam-$CaCl_2$ composite during 4 cycles of heating and cooling in the temperature range of -40 ℃ and 115 ℃ at a constant rate of 0.5 ℃/min. The onset temperature, offset temperature, and peak maximum temperature of melting and crystallization, as well as their average value for 4 heating/cooling cycles, are listed in Table 2. Fig. 3 shows that one exothermic peak with an onset temperature of 18.2 ± 0.8 ℃ during the cooling process and one endothermic peak with an onset temperature of 44.3 ± 0.2 ℃ during the heating process were detected, which corresponded to the crystallization and the melting of salt embedded in the metal foam, respectively. The onset crystallization

temperature and onset melting temperature detected is compatible with the values for calcium chloride tetrahydrate reported in the literature [59, 60]. The difference between onset crystallization temperature and onset melting temperature is defined as the supercooling degree ΔT_s of a phase change material and can be expressed by a hysteresis equation [61] :

$$\Delta T_s = T_M - T_C \quad (2)$$

where T_M and T_C are the melting and crystallization temperatures, respectively. As shown in Table 2, $\Delta T_s \approx 26$ ℃ was detected for the composite during the heating and cooling process. It is also notable that the supercooling degree of the first cycle (~ 27.5 ℃) was nearly 2 ℃ higher than that of the following cycles (~ 25.5 ℃). It is possible that during the first melting process, the salt particles were redistributed in the host matrix in a way favoring nucleation during the following cycles, for instance by revealing more open pores as well as metal foam struts, thus resulting in a lower supercooling degree [62, 63].

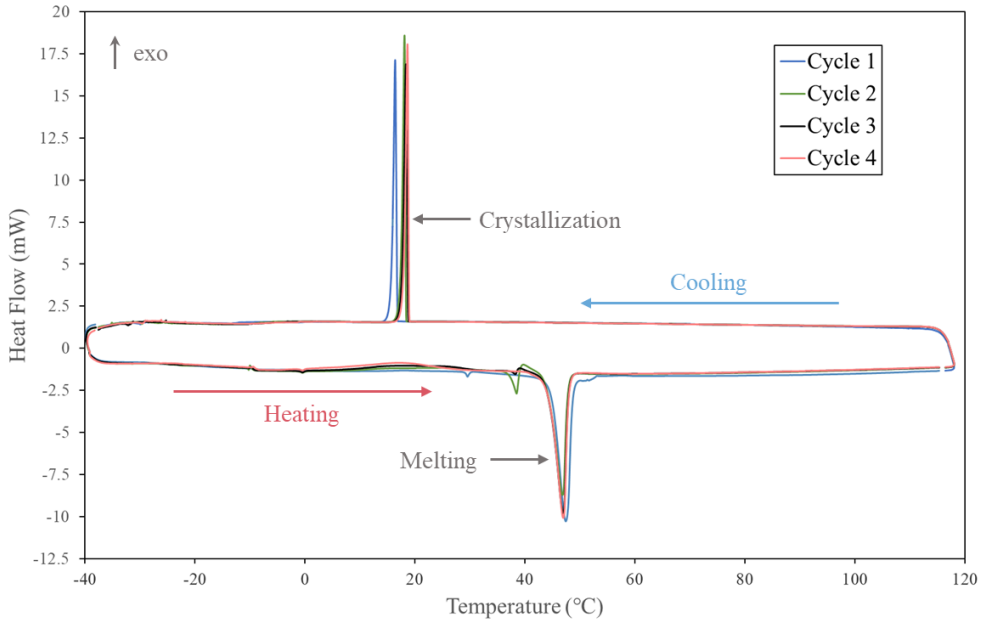

Fig. 3. DSC curves of nickel foam-salt composite during 4 cycles of heating and cooling.

It can be clearly seen in Fig. 3 that except for the first cycle, the DSC curves for the following 3 cycles are closely coincident with each other, indicating that the enthalpy of fusion and crystallization almost remained unchanged during heating and cooling cycles. In addition, the phase change temperatures were rather steady (see Table 2). These results demonstrate that the composite has sufficiently good cycling thermal reliability over a large temperature range of -40 ℃ and 120 ℃.

Cycle No.	Heating			Cooling		
	Onset T_M (℃)	T_{Peak} (℃)	Offset T_M (℃)	Onset T_C (℃)	T_{Peak} (℃)	Offset T_C (℃)
1	44.5	47.6	48.6	16.8	16.4	15.7
2	44.1	47.0	47.8	18.4	18.1	17.4
3	44.2	47.1	47.9	18.8	18.4	17.7
4	44.2	47.1	47.9	18.9	18.7	17.9
Average	44.3 ± 0.2	47.2 ± 0.2	48.1 ± 0.3	18.2 ± 0.8	17.9 ± 0.9	17.2 ± 0.9

* T_M = melting temperature, T_C = crystallization temperature, T_{Peak} = peak maximum temperature

Table 2. Thermal properties of composite by DSC cyclic tests.

3.2. Thermochemical performance during hydration/dehydration cycles

3.2.1. Analysis of long hydration/dehydration cycles

We present in Fig. 4 the typical curves of heat flow over time during the hydration/dehydration process of both composite and bulk salt powder. The curves obtained for the nickel foam-$CaCl_2$ composite and the aluminum foam- $CaCl_2$ composite had identical forms, so here we present the curves of the nickel foam-$CaCl_2$ composite as an example. In fact, it can be seen in Fig. 4 that the curves obtained for bulk salt powder and composites also have similar forms. For curves obtained during the hydration process (see Fig. 4a and c), the signal of heat flow stabilized during the first 15 min which provided us with a steady state baseline value of the heat flow ϕ_{bl} for evaluating the integration of heat flow over time. Then the humidified nitrogen entered the reaction vessel at t_i and a rapidly increasing heat flow signal was detected. The heat flow reached a maximum peak value of ϕ_p in 5-7 min and then decreased slowly over time. The circulation of humidified nitrogen was stopped at t_f when the humidification process time reached the target duration set by our experimental plan (Table 1). Then the heat flow signal dropped immediately and rapidly. It gradually stabilized near the baseline in 30 min. For the following dehydration process (see Fig. 4b and d), the dry nitrogen gas entered the reaction vessel after the signal stabilized. The circulation of dry nitrogen continued until the signal of heat flow gradually returned to the baseline. During the whole process, the temperature of the sample was controlled at 22.76 ℃.

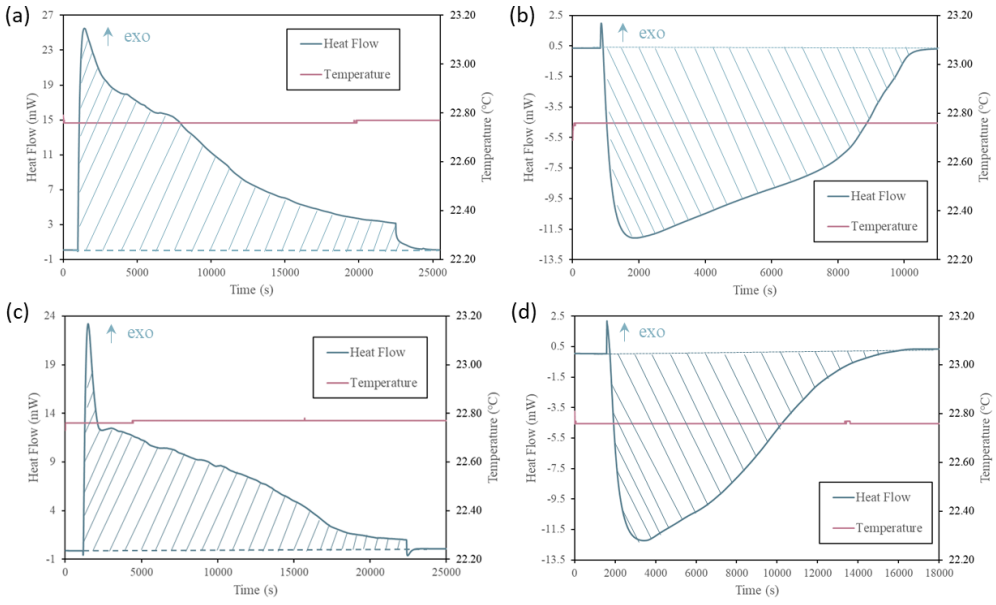

Fig. 4. Typical curves of heat flow over time during (a) hydration and (b) dehydration process of bulk calcium chloride powder and during (c) hydration and (d) dehydration process of composite (here we present the curves of nickel foam-$CaCl_2$ composite for example).

The quantity of thermal energy Q released/restored during the hydration/dehydration process is estimated as follows:

$$Q(t) = \int_{t_i}^{t_f} [\phi(t) - \phi_{bl}]dt \quad (3)$$

The normalized quantity of thermal energy Q_N released/restored during each cycle is defined as follows:

$$Q_N = \frac{Q}{m_{CaCl_2}} \quad (4)$$

where m_{CaCl_2} is the mass of $CaCl_2$ contained in each sample.

The normalized thermal energy Q_N released during 12 cyclic hydration processes (see Table 1) for bulk $CaCl_2$ salt powder, nickel foam-$CaCl_2$ composite, and aluminum foam-$CaCl_2$ composite are presented in Fig. 5. For the first cycle of 360 min hydration, the bulk $CaCl_2$ powder outperformed the other two composite significantly by reaching 1074.3 kJ/kg^{salt} in terms of thermal energy released during this time range, while for nickel foam-$CaCl_2$ composite, the value was 730.8 kJ/kg^{salt} and 811.0 kJ/kg^{salt} for aluminum foam-$CaCl_2$ composite. Yet, in the following cycles, especially from the 5th cycle, the performance of bulk $CaCl_2$ powder exhibited a clear disadvantage compared to the other two composites. For a hydration time range of 90 min (cycle N°5, 6, 7 and 8), the average Q_N released by nickel foam-$CaCl_2$ composite and by aluminum foam-$CaCl_2$ composite was 705.3 kJ/kg^{salt} and 525.7 kJ/kg^{salt}, which improved 146.1% and 83.5% respectively compared to that of bulk $CaCl_2$ powder (286.5 kJ/kg^{salt}). In the following cycles, for hydration time range of 45 min (cycle N°9, 10, 11), the advantage of composites' performances became increasingly apparent. In particular, the composite with aluminum foam as the matrix released up to 351.2 kJ/kg^{salt} for the average Q_N of these 3 cycles, which was 4.9 times more than the amount released by bulk $CaCl_2$ powder (72.0 kJ/kg^{salt}), while the nickel foam-$CaCl_2$ also released up to 4.0 times more thermal energy than the bulk salt powder, which was 288.3 kJ/kg^{salt}. Then, in the last cycle, we reproduced exactly the same experimental conditions of the first cycle, which means the samples were re-humidified for 360 min as in the first cycle, to investigate how the samples performed after 11 hydration/dehydration cycles. Results showed that nickel foam-$CaCl_2$ composite provided a Q_N of 903.9 kJ/kg^{salt}, which improved 23.7% compared to that of the first cycle, while aluminum foam-$CaCl_2$ composite provided a Q_N of 834.1 kJ/kg^{salt} in the 12th cycle, which slightly increased by 2.8% compared to the first cycle. In contrast, Q_N of bulk $CaCl_2$ powder decayed by 63.2% after 11 cycles, by providing a Q_N of only 395.8 kJ/kg^{salt} in the 12th cycle.

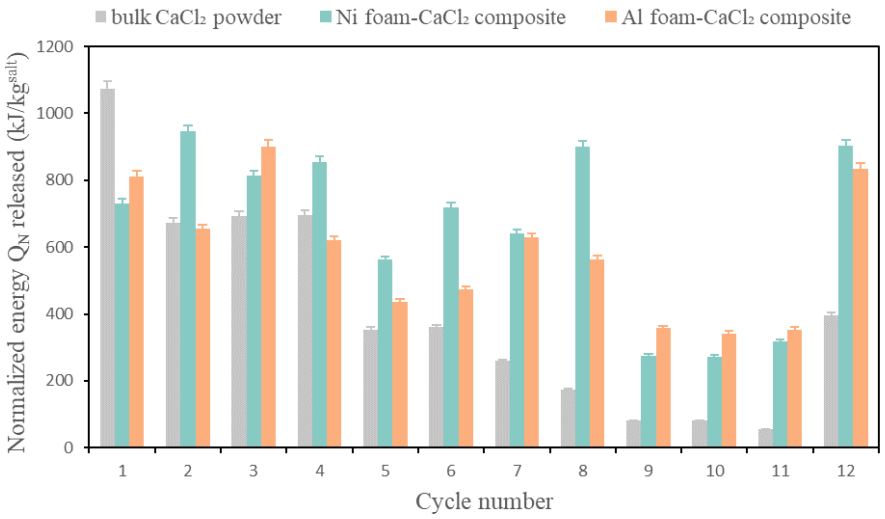

Fig. 5. Normalized thermal energy released during 12 cyclic hydration/dehydration processes of nickel foam-$CaCl_2$ composite, aluminum foam-$CaCl_2$ composite, and bulk $CaCl_2$ powder.

In order to better compare the trends in performance of these 3 kinds of samples during the 12 hydration/dehydration cycles by eliminating the influence on Q_N due to the difference in hydration time during different cycles, the values of normalized thermal energy Q_N released for each kind of sample were calculated and compared for the first 45 minutes of each humidification as presented in Fig. 6. Although bulk $CaCl_2$ powder provided the highest Q_N in the first cycle, it is clearly seen that the performance of bulk $CaCl_2$ powder decreased from the 2nd cycle and continued to decline sharply after 6 cycles, resulting in a performance degradation of 78.5% at the 12th cycle compared to the 1st cycle (from 265.6 to 57.2 kJ/kg^{salt}). While the performance of both composites was found to be much more stable. Both composites provided a lower Q_N compared to the bulk $CaCl_2$ powder in the first cycle, however, in the following cycles, the composites showed superior performance and enhanced cycling stability. After 12 cycles, Q_N improved from 179.3 to 299.6 kJ/kg^{salt} for nickel foam-$CaCl_2$ composite and from 225.6 to 346.5 kJ/kg^{salt} for aluminum foam-$CaCl_2$ composite, which indicates a 67.1% and a 53.6% increase in Q_N, respectively. Moreover, there wasn't any tendency for Q_N to degrade for both composites after these 12 cycles. The results also demonstrate that for the first 45 min of the 12th cycle, Q_N of nickel foam-$CaCl_2$ composite and of aluminum foam-$CaCl_2$ composite improved substantially to 5.2 and 6.1 times that of bulk $CaCl_2$ powder.

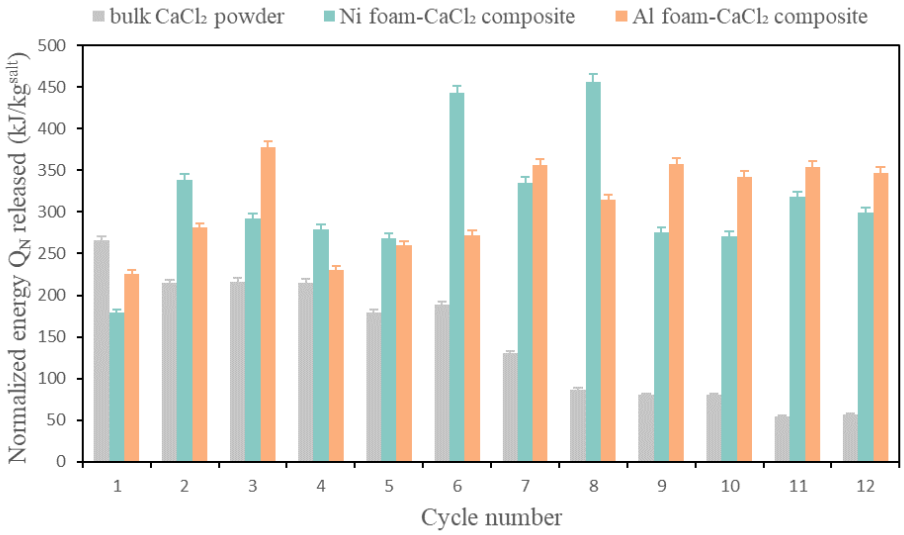

Fig. 6. Normalized thermal energy released during the first 45 min of each humidification process for 12 hydration/dehydration cycles of nickel foam-$CaCl_2$ composite, aluminum foam-$CaCl_2$ composite, and bulk $CaCl_2$ powder.

The results obtained from the long hydration/dehydration cycles provided us with fundamental data allowing for comparison of the cyclic thermal properties for bulk $CaCl_2$ powder, nickel foam-$CaCl_2$ composite, and aluminum foam-$CaCl_2$ composite.

For bulk $CaCl_2$ powder, though it provided relatively high thermal energy in the first hydration process, Q_N dropped substantially and continuously during the following humidification cycles due to deliquescence and agglomeration, inducing specific surface loss, which yielded poor cyclic stability [46, 64].

Conversely, on the one hand, for nickel foam-$CaCl_2$ composite and aluminum foam-$CaCl_2$ composite, there was no degradation in terms of Q_N after 12 cycles of hydration/dehydration.

On the other hand, surprisingly, both of them showed a significant increase in Q_N in the last and longest cycle of hydration (N°12) compared to the first longest cycle (N°1). In general, except for the first cycle, the thermal energy released by the composites compared to that by the bulk salt was substantially improved in all the rest of the cycles, and this advantage tended to increase with the number of cycles. This clearly demonstrate that the composites combining a hygroscopic salt (such as calcium chloride) dispersed in metal foam as a host matrix exhibited excellent cyclic stability and superior thermal energy storage capability compared to bulk $CaCl_2$ powder. This improvement is undoubtedly attributable to the use of the metal foam as a porous matrix, which might have preserved the salt particles from agglomeration and compaction effects related to deliquescence and swelling during hydration cycles. As a result, the metal foam matrix might have preserved the specific reaction surface and provided more efficient pathways for mass and heat transfer.

We define $\phi_{p,N}$ the normalized peak maximum heat flow during the hydration process as follows:

$$\phi_{p,N} = \frac{Max[\phi(t)]}{m_{CaCl_2}} \tag{5}$$

In the case of composites, the value of $\phi_{p,N}$ is considered to be strongly influenced by the spatial distribution, size, and morphology of salt crystals deposited in the composite. As for bulk salt, it is also considered to be influenced by the degree of dispersion and agglomeration of the salt crystals. In both cases, the value of $\phi_{p,N}$ can be seen as an implicit indicator of the heat and mass transfer efficiency of each sample. Fig. 7 illustrates the $\phi_{p,N}$ of hydration process for these three kinds of samples during 12 hydration/dehydration cycles. For all samples, the trends of $\phi_{p,N}$ were almost the same as these of the respective Q_N during hydration over 12 cycles. For the bulk salt, the average of $\phi_{p,N}$ was 64.4 W/kg^{salt} and the maximum $\phi_{p,N}$ for the 12 cycles appeared during the first hydration process. $\phi_{p,N}$ continued to decrease in the following cycles and reached by the last cycle a degradation of 73.5%, as compared to its maximum value obtained at the first cycle. This indicates that during the initial phase of the experiment, the bulk salt particles were more uniformly dispersed in the sample vessel, providing a larger specific surface area for hydration. As the cycles progressed, the bulk salt underwent deliquescence and agglomeration, resulting in a decreasing surface area and thus reducing its cycling stability in terms of Q_N, as shown in Fig. 6 and in terms of $\phi_{p,N}$, as shown in Fig. 7. For nickel foam-$CaCl_2$ composite and aluminum foam-$CaCl_2$ composite, the average of $\phi_{p,N}$ over 12 cycles were 140.2 W/kg^{salt} and 139.9 W/kg^{salt} respectively, which was about 2.2 times higher than that for the bulk salt. In addition, no evidence of $\phi_{p,N}$ degradation was detected in either composite throughout the 12 cycles and the minimum $\phi_{p,N}$ was that of the first hydration for both composites, resulting in an increase of 27.5% and 51.9% in terms of $\phi_{p,N}$ in the last cycle for nickel foam-$CaCl_2$ composite and aluminum foam-$CaCl_2$ composite, respectively.

The conclusions drawn from Fig. 7 regarding $\phi_{p,N}$ correspond well to the previous conclusions regarding Q_N, which illustrate the influence of the distribution and deposition morphology of the salt particles on the cyclic stability and energy storage properties, validating the superiority offered by open-cell metal foams as a host matrix for the composites.

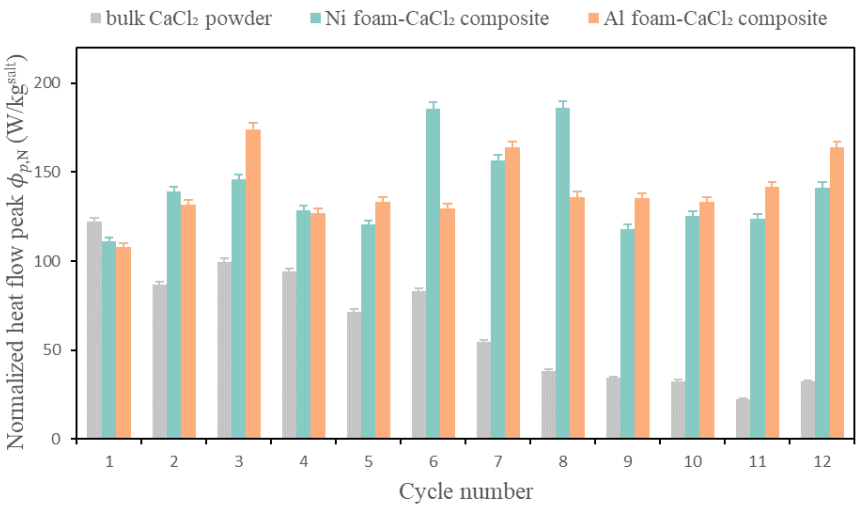

Fig. 7 Normalized peak maximum heat flow of hydration process during 12 hydration/dehydration cycles of nickel foam-$CaCl_2$ composite, aluminum foam-$CaCl_2$ composite, and bulk $CaCl_2$ powder.

These results also suggest that during the first hydration cycle, the topological parameters (spatial distribution and morphology) of the salt particles deposited in the composites have evolved in a way improving the thermochemical performances. We can also infer that if the topological evolutions continued in the following cycles, it did not affect the performances of the composites in thermochemical terms (Q_N) related to the specific reaction area, nor in kinetic terms ($\phi_{p,N}$) related to mass transfer capability, which means the portion of accessible open pores in the metal foam did not decrease during the cycles, thus leading to a better performance in terms of cyclic stability and quantity of thermal energy released.

3.2.2. Analysis of short hydration/dehydration cycles

In order to better verify the superior performance of the metal foam-$CaCl_2$ composites compared to that of bulk $CaCl_2$ salts, 2 repetition experiments were performed for each kind of sample. The experiment consisted of 6 cycles, as described in section 2.4.2, where the samples were humidified for 45 minutes per cycle with other experimental conditions remaining unchanged, and the normalized thermal energy Q_N released during the process was then calculated and analyzed. Experimental errors were analyzed according to the data acquired through repetition tests.

Fig. 8 illustrates that from the 2nd cycle onwards for both composites Q_N was significantly higher than that of bulk $CaCl_2$ powder. For cycle N°2 to N°6, the improvement of normalized thermal energy Q_N released by aluminum foam-$CaCl_2$ composite to bulk $CaCl_2$ powder was between 77.9% to 129.6%, while for nickel foam-$CaCl_2$ composite, the improvement was between 54.5% to 85.9% (see Fig. 9). For nickel foam-$CaCl_2$ composite, Q_N varied from 256.7 kJ/kg^{salt} (N°1) to 314.3 kJ/kg^{salt} (N° 6), which increased by 22.4%, with the highest Q_N appeared in the 4th cycle (323.2 kJ/kg^{salt}). As for aluminum foam-$CaCl_2$ composite, Q_N increased from 299.3 kJ/kg^{salt} (N°1) to the highest of 389.5 kJ/kg^{salt} (N°6), achieving an improvement of 30.1%. In general, the results confirm an improved cyclic stability of the composites in comparison with bulk $CaCl_2$ powder. After the first hydration, it can be seen that for both composites Q_N stabilized or slightly increased, while it decreased for bulk $CaCl_2$ powder. These opposite evolutions relate to microstructural changes of the reactive material

which we will further discuss in section 3.3.

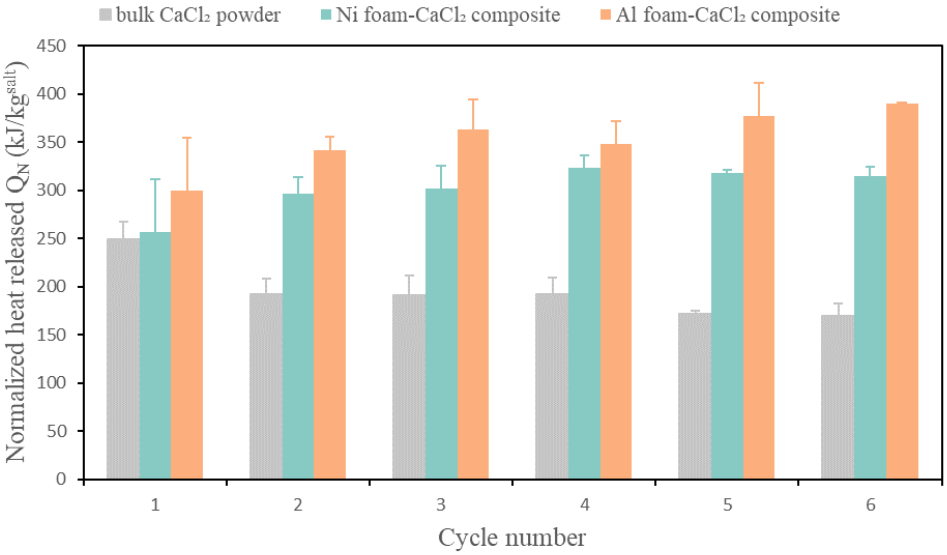

Fig. 8. Normalized thermal energy released during 6 short hydration/dehydration cycles (45 min hydration) of nickel foam-$CaCl_2$ composite, aluminum foam-$CaCl_2$ composite, and bulk $CaCl_2$ powder.

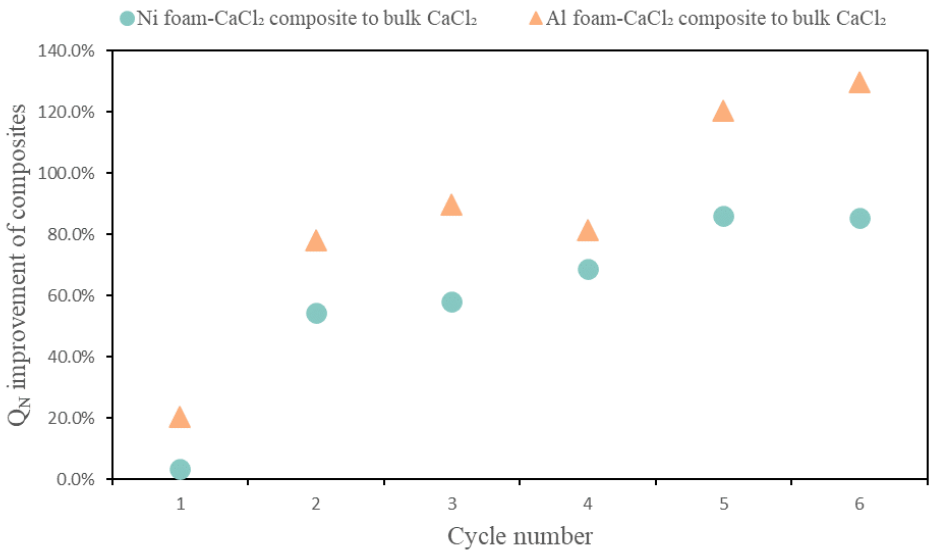

Fig. 9. Q_N improvement of composites compared to bulk $CaCl_2$ powder during 6 short hydration/dehydration cycles.

The results of the short hydration/dehydration cycle experiments once again verified the superior quantity of thermal energy stored/released and enhanced cycling stability of composites compared to bulk salt powder under the same experimental conditions. Compared to the previous experimental results concerned with long cycles, we found that after the first cycle of hydration, the bulk salt did not show strong degradation of performances during the short hydration/dehydration cycles. This observation is consistent with time-dependent microstructural evolution, related to the swelling of hydrated salt crystallites and corresponding agglomeration/compaction, which naturally depends on the number and duration of cycles.

For the composites, we found performance trends similar to those shown during the long

cyclic process (Fig. 6). In both cyclic processes, the Q_N was minimum for the first cycle, then increased for the following. It is therefore presumed that the metal foam-salt composites need a certain duration of time to optimize their thermochemical properties. This time-lapse represents a maturation period, during which the microstructure evolves owing to topological changes concerning salt hydrate deliquescence, swelling, agglomeration, and local redistribution within the metallic foam.

This interpretation is strengthened by the fact that the thermal energy released during the first hydration of the composites varied relatively widely for different samples under the same experimental conditions. For example, the error in Q_N of the first hydration was 21.5% for the nickel foam-$CaCl_2$ composite and 18.4% for the aluminum foam-$CaCl_2$ composite. Conversely, during the subsequent cycles, the error for different samples decreased considerably and the thermochemical properties became relatively stable. The larger differences in thermochemical performances during the initial hydration might be due to differences in the initial distribution of salt crystallites in the metal foam, resulting from the preparation process. Such differences are expected to vanish after the maturation period of the first hydration, owing to salt hydrate deliquescence redistribution within the metallic foam network.

In section 3.3, we will specifically address the possible reasons and explanations for the superior performance and the enhanced cyclic stability of the designed composites by characterization based on in situ ESEM hydration/dehydration cycling test.

3.2.3. Apparent energy density of Ni/Al foam-$CaCl_2$ composite

In this part, the apparent energy density of two kinds of metal foam-$CaCl_2$ composites using nickel foam and aluminum foam are compared. We define the apparent energy density E_d as follows:

$$E_d = \frac{Q}{V_{sample}} \tag{6}$$

where Q is the quantity of thermal energy released/restored during the hydration/dehydration process as defined in equation (3) and V_{sample} is the total volume of the composite sample.

Fig. 10 presents the energy density of both composites in hydration/dehydration cycles. It is clear that the E_d of nickel foam-$CaCl_2$ (48.5 wt%) composite exceeded that of aluminum foam-$CaCl_2$ (21.0 wt%) composite in both long and short hydration/dehydration cycles (experimental procedure described in section 2.4.2). In long hydration/dehydration cycles (as shown in Fig. 10a), as hydration duration Δt_{hydr} differed from 45 min to 360 min for different cycles, the E_d of Ni foam-$CaCl_2$ composite was between 82.3 MJ/m^3 (N°10 - Δt_{hydr} of 45 min) and 286.9 MJ/m^3 (N°2 - Δt_{hydr} of 180 min), while the E_d of Al foam-$CaCl_2$ composite was between 78.5 MJ/m^3 (N°10 - Δt_{hydr} of 45 min) and 206.8 MJ/m^3 (N°3 - Δt_{hydr} of 180 min). During the 12th cycle (Δt_{hydr} of 360 min), Ni foam-$CaCl_2$ composite provided a E_d of 274.2 MJ/m^3, improved by 43% compared to that of Al foam-$CaCl_2$ composite, which provided a E_d of 191.5 MJ/m^3. The results of short cycles (Δt_{hydr} of 45 min) shown in Fig. 10b once again confirmed the superiority of Ni foam-$CaCl_2$ composite over Al foam-$CaCl_2$ composite in terms of energy density. E_d provided by Ni foam-$CaCl_2$

composite was between 76.6 MJ/m^3 (N°1) and 96.4 MJ/m^3 (N°4), with an average E_d of 90.0 MJ/m^3 for 6 cycles. While E_d provided by Al foam-$CaCl_2$ composite was between 65.8 MJ/m^3 (N°1) and 84.6 MJ/m^3 (N°6), with an average E_d of 76.8 MJ/m^3 for 6 cycles. An improved E_d of 17% was obtained for Ni foam-$CaCl_2$ composite compared to Al foam-$CaCl_2$ composite for 6 cycles of hydration/dehydration process with Δt_{hydr} of 45 min for each cycle. The summary of E_d of both composites for all cycles are shown in Table 3.

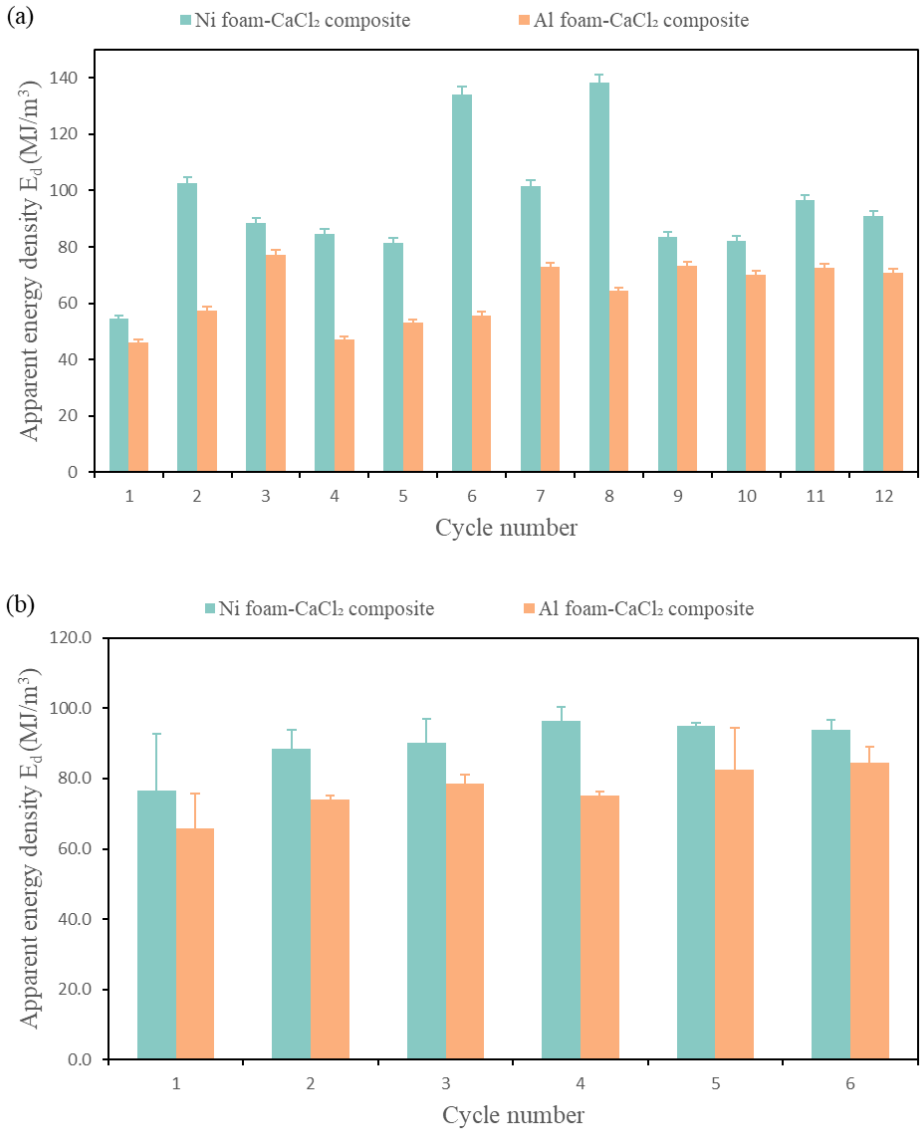

Fig. 10. Energy density of nickel foam-$CaCl_2$ composite and aluminum foam-$CaCl_2$ composite in (a) 12 hydration/dehydration cycles of different hydration duration and (b) 6 hydration/dehydration cycles of 45 min hydration duration.

Obviously, the difference in apparent energy density of these two composites meanly derives from the different morphology and microstructure of the host matrix (metal foam), especially the porosity. The porosity of nickel foam used is about 96%, while the porosity is about 40% for aluminum foam. The difference in porosity greatly affected the content of salt deposited in the metal foam, thus affecting the apparent energy density.

From the perspective of cyclic stability and thermochemical energy density, the most effective thermochemical composite is the nickel foam-$CaCl_2$. Such composite, based on

nickel foam as host matrix offers the highest porosity proportion as well as appropriate pore size and would be a promising choice for thermochemical heat storage systems. However, the source, cost, and mechanical properties should also be taken into account. Not to mention the corrosion problem of metal [65-67]. These aspects still need further exploration.

Cycle No.	Apparent energy density E_d (MJ/m^3)			
	Ni foam-$CaCl_2$ composite		Al foam-$CaCl_2$ composite	
	Long cycle	Short cycle*	Long cycle	Short cycle*
1	221.7	76.6	186.2	65.8
2	286.9	88.4	150.4	74.0
3	246.8	90.1	206.8	78.5
4	259.0	96.4	142.3	75.3
5	170.4	94.9	100.1	82.4
6	218.4	93.7	108.8	84.6
7	194.1	-	144.3	-
8	272.8	-	129.5	-
9	83.6	-	82.1	-
10	82.3	-	78.5	-
11	96.5	-	81.3	-
12	274.2	-	191.5	-

*Average value calculated from repetition tests.

Table 3 Apparent energy density results of both composites for all cycles.

3.3. Performance improvement mechanism of composites

In this section, we present results obtained during hydration/dehydration cycling tests, performed with in situ ESEM, in order to investigate the topological behavior of salt hydrates in the composite. The aim is to observe possible redistribution of salt during hydration processes and to provide explanations for the performance improvement in terms of cyclic stability and quantity of thermal energy released during hydration of metal foam-salt composites compared to bulk salt powder.

As introduced in section 2.5, the experimental conditions of cyclic hydration/dehydration tests performed in the differential scanning calorimeter were reproduced during in situ ESEM observation with images recorded every 5 seconds. Fig. 11 illustrates the continuous evolution of the sample surface as the relative humidity increased from 0 to approximately 54% under an isothermal condition for the nickel foam-$CaCl_2$ composite. In the region of interest (ROI) presented in Fig. 11, it is clearly seen that not all the open pore spaces of the metal foam matrix were filled with salt at the initial state, which ensured that the water vapor could pass smoothly through the metal foam and thus come into contact with the salt crystallites distributed within the metal foam, thereby promoting the hydration process and releasing the thermal energy. Besides the open pores of the metal foam, we observed the entrapped salt particles at the initial state with 0.4% RH, where the cross-sections of the metal foam struts protruding from the salt layer were also clearly visible, as shown in Fig. 11a. By adjusting the chamber pressure, we control the relative humidity for the hydration and dehydration process. As the hydration process began, the salt on the surface of the sample gradually absorbed water with increasing humidity. When the RH reached about 45%, we observed the part of the salt layer denoted by the dashed line shrieked and formed a hole (see Fig. 11b). This hole formed on the surface salt layer continued to expand as the RH increased to 51.4% (see the part circled by the dashed line in Fig. 11c). When the relative humidity reached 54.7%, which was approximately the same condition as in the cyclic hydration/dehydration tests for thermal

analysis (54% RH), we stopped raising the vapor pressure in the SEM chamber. The sample was kept under this condition for about 30 minutes, during which no further changes in the ROI were detected. Fig. 11d showed that compared to lower RH conditions, the hole in the salt layer continued expanding before the RH reached 54.7%, which is also indicated by the higher proportion of metal foam struts that can be observed under the surface salt layer compared to the former states. As no further changes in the ROI were detected under this condition for 30 min, it may be considered that the hydration reaction was completed and the subsequent redistribution of salt hydrates within the metallic foam network has been achieved. This suggests that once a certain hydration degree is reached, the redistribution and relocation process of the surface salt layer stops. This in turn means that hydration kinetics are very fast and may be achieved within a few minutes.

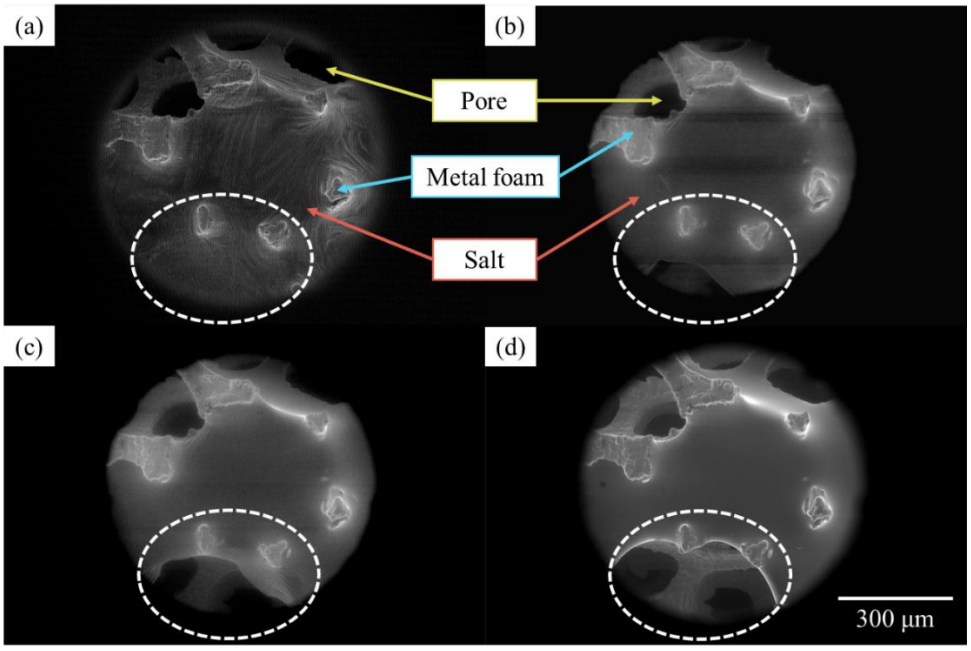

Fig. 11. GSED images (x107 magnification) of the nickel foam-$CaCl_2$ composite sample surface with the relative humidity increasing from (a) 0.4%, (b) 45.3%, (c) 51.4%, to (d) 54.7% under isothermal condition. The redistribution of salt during the variation of humidity is circled in a dashed line.

A different nickel-based composite was observed at higher magnification, with a smaller horizontal field width (HFW) of 250 μm chosen as the region of interest (ROI), in order to focus on the evolution of the interfaces between the metal foam and the salt layer during hydration/dehydration cycles (Fig. 12). At the initial state with a relative humidity of 0.4%, as shown in Fig. 12a, a layer of dry salt crystals could be observed tightly surrounding the strut of the metal foam. The fine fissures formed during sample preparation and drying for preservation were visible on the surface of the salt layer. At this point, there were no observable open pores of the metal foam in the ROI. Then the vapor pressure was raised in the SEM chamber for the relative humidity to increase. During the increase of relative humidity, the deliquescence of the salt was observed at approximately 30% RH, which is in accordance with the deliquescence relative humidity (DRH) of hexahydrate ($CaCl_2 \cdot 6H_2O$) at about 23 ℃[68-70]. Fig. 12b illustrates the ROI after 30 min's stabilization when RH reached 54.7%. In this figure, the deliquescence of the salt layer after the first hydration process can be clearly seen. It is also worth noting in Fig. 12b that the salt which was originally located in the left area of the ROI, surrounding the strut of metal foam, separated from it along the struts

and redistributed in the host matrix, thus forming a hole in the salt layer revealing the original pores and struts of metal foam (see the part marked in circle). In the next step, the relative humidity was reduced to 0.4% then remained at this RH for 30 min to dry the samples. As shown in Fig. 12c, the salt layer that still surrounded the struts of the metal foam after the first hydration process dehydrated and formed a salt layer with a thickness gradient. Compared to Fig. 12b, the hole formed during the first hydration process remained unchanged (the part marked in circle) and no additional holes in the salt layer were formed in the ROI during this process. The second hydration cycle was then carried out and the ROI after the second hydration process is presented in Fig. 12d. It can be clearly seen that the salt layer was again deliquescent, allowing the salt to flow in the metal foam either along the struts or through the pores. The change in the thickness of the salt layer in the ROI allowed us to see the shape of the metal foam strut (see the mark in blue dashed lines in Fig. 12d). Most notably, another hole was formed in the salt layer in the upper part of the ROI (marked in circles in Fig. 12d), indicating that the salt layer continued to relocate in the metal foam matrix during this second hydration process, as was observed during the first hydration process (shown in Fig. 12b).

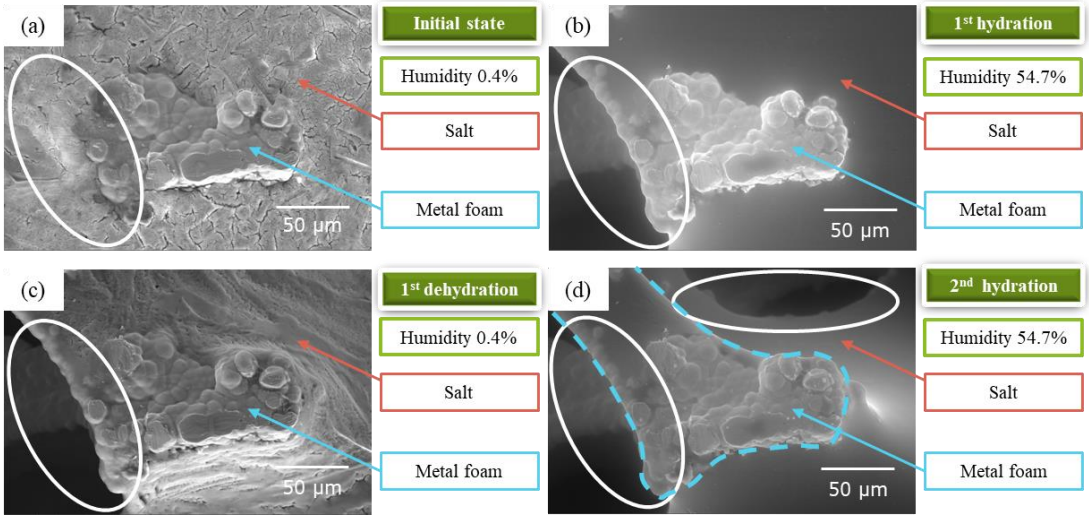

Fig. 12. GSED images (x508 magnification) of the nickel foam-$CaCl_2$ composite sample surface during 2 hydration/dehydration cycles with (a) the initial state (0.4% RH), (b) after first hydration (54.7% RH), (c) after first dehydration (0.4% RH) and (d) after second hydration (54.7% RH) under isothermal condition. The redistribution of salt during the hydration/dehydration cycles is marked in circle.

Observations from in situ hydration/dehydration cycle tests on nickel foam-$CaCl_2$ composites show that after sample preparation and drying process, the salt tended to be deposited surrounding the struts of the metal foam pores or in the metal foam cells. The distribution of salt crystallites was irregular, some of the pores of the metal foam were filled, while others remained open. During the hydration process at a constant temperature (approximately 23°C), $CaCl_2$ became deliquescent when the relative humidity reached about 30%. The resulting gel-like salt flowed along the struts driven by surface tension forces and hence redistributed homogeneously in the metal foam. Most importantly, the redistribution favored restoring the open porosity. According to observation, this reorganization mechanism of the salt may be activated during each hydration process. It can also be inferred that as the number of hydration/dehydration cycles increases, the distribution of salt in the metal foam matrix tends to homogenize the salt dispersion along the metal foam struts, hence reaching a stable topology, with an optimum surface to volume ratio and preserving the interconnections of the

foam porosity.

By observing at different scales, it is noted that not all the deliquescent salt necessarily redistributes during the first hydration process, as shown in Fig. 13. By comparing the initial state (Fig. 13a) and the state after the first hydration process (Fig. 13b), it is clearly observed that the salt completely embedded in a small cell (< 200 μm) remained trapped even after hydration and deliquescence. This local behavior is contrasting with observations shown in Fig. 11, where the deliquescent salt massively migrated from a larger cell (> 300 μm). However, the smaller cell in Fig. 13 was nearly complete and offered only a cell window to the observation surface, while the large pore shown in Fig. 11 was incomplete and largely opened to the observation surface. These observations indicate the strong role of capillary effects and suggest that the local structure of the foam will control the actual salt redistribution. This aspect highlights the microstructural importance of the metal foam, for instance, the size and the size distribution of the metal foam cells, or the size of the struts and cell windows.

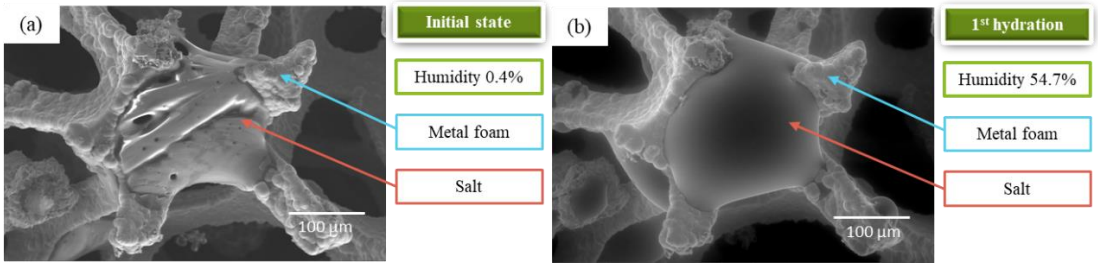

Fig. 13. GSED images (x254 magnification) of the nickel foam-$CaCl_2$ composite sample surface focused on the interface of salt and metal foam with (a) the initial state (0.4% RH) and (b) after first hydration (54.7% RH).

The conclusions obtained from observations during the in situ hydration/dehydration cycling test give a reasonable explanation and a possible mechanism for the improvements of the composites compared to bulk salt in terms of thermochemical performance. The enhanced performance of the metal foam-salt composite can be partially attributed to the porous structure of the metal foam. On the one hand, the porous matrix serves for salt deposition. On the other hand, the open pores increase the specific reaction area, which facilitates mass and heat transfer while effectively avoiding the degradation of performance due to salt swelling and agglomeration. What's more, thanks to the pore size of the selected metal foam and the proportion of free pores after each cycle, the host matrix ensures that the salt can be relocated and reorganized in the composite even if agglomeration or even deliquescence occurs, which greatly enhances its cyclic stability as well as the mass and heat transfer efficiency. The composite offers a dynamic microstructure, with local topological evolutions during hydration cycles, while allowing the maintenance of statistically stable proportions of interconnected open pores and specific reaction areas. In this case, the global thermochemical performances might remain stable over time. Without the metal foam serving as host matrix, the cyclically swelling salt crystallites would undoubtedly lead to progressive compaction, with loss of open porosity and specific reaction area, which would lead to progressively decreasing thermochemical performances. Actually, these contrasting scenarios for composites and bulk salt powder are wholly supported by our thermochemical measurements (section 3.2).

The observations from the in situ experiments can also explain some of the conclusions drawn from the thermal analysis experiments related to composite performance. In section 3.2, results suggested that for both composites the minimum value of the normalized thermal

energy released Q_N during cycles usually occurred at the first hydration process and tended to increase and stabilize in the subsequent cycles. Meanwhile, the experimental data presented in section 3.2.2 showed relatively large errors in Q_N of the first hydration process for both composites during repetition tests on different samples. Based on the in situ ESEM observations, this is possibly due to the differences in the position of salt deposited on the surface of the sample during the preparation and drying process, as well as the percentage of free open pores remaining in the composite after salt deposition. All these factors resulted in a greater variation in performance exhibited by the initial hydration process for different samples. However, as seen in the in situ hydration/dehydration experiment, salts without sufficient structural support provided by the initial deposition location are more likely to relocate after the first cycle of hydration. It can be presumed that as the hydration/dehydration cycle continues, salts continue to relocate and reorganize, thus resulting in a more dispersed and rational deposition in the composite, which increases the specific surface area while leaving more pathways for heat and mass transfer, thus improving and gradually stabilizing the performance of the composites after the first hydration. This mechanism well explained the experimental results mentioned in 3.2, where Q_N was usually at a minimum during the first hydration cycle, and the reduction of the experimental error in the different samples to a reasonable range after a few cycles. This also confirms our conjecture based on the results of the thermal experiments, that the first cycle can be considered as an activation (or maturation) cycle, allowing for an optimum salt redistribution, hence ensuring the most effective salt topology in terms of the specific reaction area, which in turn ensures the stability of the thermochemical heat capacity during further cycling.

In addition, the metallic framework of the metal foam provides improved thermal conductivity and mechanical strength to the overall system. All of the above results indicate that the metal foam-salt hydrate composite introduced in this paper is a suitable and promising thermochemical material.

4. Conclusion

To overcome the drawbacks of pure calcium chloride as thermochemical material, this study presented a newly designed metal foam-salt hydrate composite consisting of open-cell metal foam with a pore size of 350 μm as host matrix and calcium chloride as hygroscopic salt dispersed in the pores for thermochemical heat storage. The aim was to investigate the feasibility of the newly designed composite as a TCM and to compare its performance with that of pure calcium chloride. The main results are shown as follows:

(1) A method for dispersion of salt in open-cell metal foam was developed using an oversaturated salt solution and by immersing the metal foam sample in. Intensive and continuous stirring was required to achieve an even distribution of salt. The composite sample should be kept in the oven for more than 48 h at 90 °C before experiments.

(2) Metal foam-salt composites showed significant improvement in terms of cyclic stability and quantity of thermal energy released/stored compared to bulk calcium chloride in both long and short hydration/dehydration cycles. For cyclic stability, composites presented a slight increase and stabilization of thermal energy released upon cycles, while salt showed substantial and continuous degradation in performance. For heat released during hydration, composites outperformed considerably the bulk calcium chloride in all cycles, except for the

first cycle, which may be considered as an activation cycle allowing to reach the optimum composite microstructure. The result also indicated that for discharging/charging the same amount of thermal energy, metal foam-salt composites were more efficient than bulk calcium chloride.

(3) Nickel foam-$CaCl_2$ composite provided better performance in terms of apparent energy density as compared to aluminum foam-$CaCl_2$ composite. The difference in energy density of these two composites meanly derives from the different porosity of the host matrix (96% for nickel foam, 40% for aluminum foam). The difference in porosity greatly affects the salt content deposited in the metal foam, thus affecting the energy density.

(4) After confirming the feasibility of the designed metal foam-salt composite as TCM and its improvement in thermochemical performance compared to that of bulk salt powder, the performance enhancement mechanism of the composite was investigated by in situ ESEM hydration/dehydration cycling test. The observation indicated that the open-cell metal foam with a pore size of 350 μm provided sufficient salt deposition sites, allowing the salt to be relocated and reorganized in the metal foam cells even after deliquescence during the hydration process while preventing the swelling and agglomeration of salt, which effectively increased the cyclic stability of the composite. In addition, large open volumes and multiple flow paths provided by the metal foam increased the specific reaction surface, favored heat and mass transfer, and ensured no volume change even if swelling and agglomeration of salt occurred. Moreover, metal foam provided high thermal conductivity. All of the above-mentioned advantages led to a significant improvement in the thermochemical performance of the composite compared to that of bulk salt powder.

In conclusion, the metal foam-salt hydrate composite developed in our work is suitable and promising for thermochemical energy storage, offering both mechanical and thermochemical advantages. On the one hand, the metallic foam ensures structural integrity allowing for flexible industrial handling of thermochemical storage units. On the other hand, the metal foam guarantees the microstructural stability of the reactive material, hence preserving an economically durable life span of the composite. At last, the thermochemical composites presented in this work have a low environmental footprint. The reactive salt hydrates are environmentally friendly and allow for total recycling along with the metal foam. Moreover, this work helps to open up innovative possibilities for research in sorption thermal energy storage systems and also helps to understand the thermochemical performance improvement mechanism of the composite thermochemical material.

Acknowledgments

This research was produced within the framework of Energy4Climate Interdisciplinary Center (E4C) of IP Paris and Ecole des Ponts ParisTech. This research was supported by 3rd Programme d'Investissements d'Avenir [ANR-18-EUR-0006-02] and by the Foundation of Ecole Polytechnique (Chaire "Défis Technologiques pour une Énergie Responsable" financed by TotalEnergies).

References

[1] IEA(2022), *Renewables 2022*, IEA, Paris, https://www.iea.org/reports/renewables-2022, License: CC BY 4.0.
[2] IEA(2022), *World Energy Outlook 2022*, IEA, Paris, https://www.iea.org/reports/world-energy-outlook-2022, License: CC BY 4.0 (report); CC BY NC SA 4.0 (Annex A).
[3] Aydin, D., S.P. Casey, and S. Riffat, *The latest advancements on thermochemical heat storage systems*. Renewable and Sustainable Energy Reviews, 2015. **41**: p. 356-367. https://doi.org/10.1016/j.rser.2014.08.054.
[4] Donkers, P., et al., *A review of salt hydrates for seasonal heat storage in domestic applications.* Applied energy, 2017. **199**: p. 45-68. https://doi.org/10.1016/j.apenergy.2017.04.080.
[5] Weinstein, L.A., et al., *Concentrating solar power*. Chemical Reviews, 2015. **115**(23): p. 12797-12838. https://doi.org/10.1021/acs.chemrev.5b00397.
[6] Fernández, A., et al., *Selection of materials with potential in sensible thermal energy storage.* Solar energy materials and solar cells, 2010. **94**(10): p. 1723-1729. https://doi.org/10.1016/j.solmat.2010.05.035.
[7] Kuravi, S., et al., *Thermal energy storage technologies and systems for concentrating solar power plants.* Progress in Energy and Combustion Science, 2013. **39**(4): p. 285-319. https://doi.org/10.1016/j.pecs.2013.02.001.
[8] Parameshwaran, R., et al., *Sustainable thermal energy storage technologies for buildings: a review*. Renewable and Sustainable Energy Reviews, 2012. **16**(5): p. 2394-2433. https://doi.org/10.1016/j.rser.2012.01.058.
[9] Khare, S., et al., *Selection of materials for high temperature latent heat energy storage.* Solar energy materials and solar cells, 2012. **107**: p. 20-27. https://doi.org/10.1016/j.solmat.2012.07.020.
[10] Wentworth, W. and E. Chen, *Simple thermal decomposition reactions for storage of solar thermal energy*. Solar Energy, 1976. **18**(3): p. 205-214. https://doi.org/10.1016/0038-092X(76)90019-0.
[11] Wu, J. and X.F. Long, *Research progress of solar thermochemical energy storage.* International Journal of Energy Research, 2015. **39**(7): p. 869-888. https://doi.org/10.1002/er.3259.
[12] Cabeza, L.F., A. Solé, and C. Barreneche, *Review on sorption materials and technologies for heat pumps and thermal energy storage.* Renewable Energy, 2017. **110**: p. 3-39. https://doi.org/10.1016/j.renene.2016.09.059.
[13] Ma, Z., H. Bao, and A.P. Roskilly, *Electricity-assisted thermochemical sorption system for seasonal solar energy storage.* Energy Conversion and Management, 2020. **209**: p. 112659. https://doi.org/10.1016/j.enconman.2020.112659.
[14] Aydin, D., Z. Utlu, and O. Kincay, *Thermal performance analysis of a solar energy sourced latent heat storage.* Renewable and Sustainable Energy Reviews, 2015. **50**: p. 1213-1225. https://doi.org/10.1016/j.rser.2015.04.195.
[15] Linder, M., *Using thermochemical reactions in thermal energy storage systems*, in *Advances in Thermal Energy Storage Systems*. 2021, Elsevier. p. 477-495.
[16] Michel, B., P. Neveu, and N. Mazet, *Comparison of closed and open thermochemical processes, for long-term thermal energy storage applications.* Energy, 2014. **72**: p. 702-716. https://doi.org/10.1016/j.energy.2014.05.097.
[17] Carrillo, A.J., et al., *Solar Energy on Demand: A Review on High Temperature Thermochemical Heat Storage Systems and Materials*. Chemical Reviews, 2019. **119**(7): p. 4777-4816. https://doi.org/10.1021/acs.chemrev.8b00315.
[18] Yu, N., R.Z. Wang, and L.W. Wang, *Sorption thermal storage for solar energy*. Progress in Energy and Combustion Science, 2013. **39**(5): p. 489-514. https://doi.org/10.1016/j.pecs.2013.05.004.
[19] Sögütoglu, L.C., et al., *In-depth investigation of thermochemical performance in a heat battery: Cyclic analysis of K2CO3, MgCl2 and Na2S.* Applied Energy, 2018. **215**: p. 159-173. https://doi.org/10.1016/j.apenergy.2018.01.083.
[20] Marias, F., et al., *Thermodynamic analysis and experimental study of solid/gas reactor operating in open mode.* Energy, 2014. **66**: p. 757-765.

https://doi.org/10.1016/j.energy.2014.01.101.
[21] Houben, J., et al., *K2CO3 in closed heat storage systems.* Renewable Energy, 2020. **166**: p. 35-44. https://doi.org/10.1016/j.renene.2020.11.119.
[22] Pathak, A.D., et al., *A DFT-based comparative equilibrium study of thermal dehydration and hydrolysis of CaCl2 hydrates and MgCl2 hydrates for seasonal heat storage.* Physical Chemistry Chemical Physics, 2016. **18**(15): p. 10059-10069. https://doi.org/10.1039/C6CP00926C.
[23] Mamani, V., et al., *Industrial carnallite-waste for thermochemical energy storage application.* Applied Energy, 2020. **265**: p. 114738. https://doi.org/10.1016/j.apenergy.2020.114738.
[24] Michel, B. and M. Clausse, *Design of thermochemical heat transformer for waste heat recovery: Methodology for reactive pairs screening and dynamic aspect consideration.* Energy, 2020. **211**: p. 118042. https://doi.org/10.1016/j.energy.2020.118042.
[25] Girnik, I.S., et al., *Composite "LiCl/MWCNT/PVA" for adsorption thermal battery: Dynamics of methanol sorption.* Renewable and Sustainable Energy Reviews, 2020. **123**: p. 109748. https://doi.org/10.1016/j.rser.2020.109748.
[26] Sögütoglu, L.-C., et al., *Understanding the Hydration Process of Salts: The Impact of a Nucleation Barrier.* Crystal Growth & Design, 2019. **19**(4): p. 2279-2288. https://doi.org/10.1021/acs.cgd.8b01908.
[27] Tatsidjodoung, P., N. Le Pierrès, and L. Luo, *A review of potential materials for thermal energy storage in building applications.* Renewable and Sustainable Energy Reviews, 2013. **18**: p. 327-349. https://doi.org/10.1016/j.rser.2012.10.025.
[28] Li, W., et al., *Salt hydrate–based gas-solid thermochemical energy storage: Current progress, challenges, and perspectives.* Renewable and Sustainable Energy Reviews, 2022. **154**: p. 111846. https://doi.org/10.1016/j.rser.2021.111846.
[29] Lu, Z.S., et al., *Performance analysis of an adsorption refrigerator using activated carbon in a compound adsorbent.* Carbon, 2006. **44**(4): p. 747-752. https://doi.org/10.1016/j.carbon.2005.09.016.
[30] Wang, L.W., R.Z. Wang, and R.G. Oliveira, *A review on adsorption working pairs for refrigeration.* Renewable and Sustainable Energy Reviews, 2009. **13**(3): p. 518-534. https://doi.org/10.1016/j.rser.2007.12.002.
[31] Aristov, Y.I., et al., *A family of new working materials for solid sorption air conditioning systems.* Applied Thermal Engineering, 2002. **22**(2): p. 191-204. https://doi.org/10.1016/S1359-4311(01)00072-2.
[32] Aristov, Y.I., et al., *Selective water sorbents for multiple applications, 10. Energy storage ability.* Reaction Kinetics and Catalysis Letters, 2000. **69**: p. 345-353. https://doi.org/10.1023/A:1005616420331.
[33] Frazzica, A., et al., *Development of "salt in porous matrix" composites based on LiCl for sorption thermal energy storage.* Energy, 2020. **208**: p. 118338. https://doi.org/10.1016/j.energy.2020.118338.
[34] Courbon, E., et al., *A new composite sorbent based on SrBr2 and silica gel for solar energy storage application with high energy storage density and stability.* Applied Energy, 2017. **190**: p. 1184-1194. https://doi.org/10.1016/j.apenergy.2017.01.041.
[35] Zhang, Y.N., et al., *Development and thermochemical characterizations of vermiculite/SrBr2 composite sorbents for low-temperature heat storage.* Energy, 2016. **115**: p. 120-128. https://doi.org/10.1016/j.energy.2016.08.108.
[36] Sutton, R.J., et al., *Characterising the discharge cycle of CaCl2 and LiNO3 hydrated salts within a vermiculite composite scaffold for thermochemical storage.* Energy and Buildings, 2018. **162**: p. 109-120. https://doi.org/10.1016/j.enbuild.2017.11.068.
[37] Permyakova, A., et al., *Design of salt–metal organic framework composites for seasonal heat storage applications.* Journal of Materials Chemistry A, 2017. **5**(25): p. 12889-12898. https://doi.org/10.1039/C7TA03069J.
[38] Zhang, Y.N., R.Z. Wang, and T.X. Li, *Thermochemical characterizations of high-stable activated alumina/LiCl composites with multistage sorption process for thermal storage.* Energy, 2018. **156**: p. 240-249. https://doi.org/10.1016/j.energy.2018.05.047.

[39] Ejeian, M., A. Entezari, and R.Z. Wang, *Solar powered atmospheric water harvesting with enhanced LiCl /MgSO4/ACF composite*. Applied Thermal Engineering, 2020. **176**: p. 115396. https://doi.org/10.1016/j.applthermaleng.2020.115396.
[40] Mahon, D., et al., *Feasibility study of MgSO4 + zeolite based composite thermochemical energy stores charged by vacuum flat plate solar thermal collectors for seasonal thermal energy storage*. Renewable Energy, 2020. **145**: p. 1799-1807. https://doi.org/10.1016/j.renene.2019.05.135.
[41] Xu, J.X., et al., *High energy-density multi-form thermochemical energy storage based on multi-step sorption processes*. Energy, 2019. **185**: p. 1131-1142. https://doi.org/10.1016/j.energy.2019.07.076.
[42] Casey, S.P., et al., *Salt impregnated desiccant matrices for 'open' thermochemical energy storage—Hygrothermal cyclic behaviour and energetic analysis by physical experimentation.* Energy and Buildings, 2015. **92**: p. 128-139. https://doi.org/10.1016/j.enbuild.2015.01.048.
[43] Grekova, A.D., L.G. Gordeeva, and Y.I. Aristov, *Composite "LiCl/vermiculite" as advanced water sorbent for thermal energy storage*. Applied Thermal Engineering, 2017. **124**: p. 1401-1408. https://doi.org/10.1016/j.applthermaleng.2017.06.122.
[44] Zhao, Q., et al., *Optimization of thermochemical energy storage systems based on hydrated salts: A review*. Energy and Buildings, 2021. **244**: p. 111035. https://doi.org/10.1016/j.enbuild.2021.111035.
[45] Gordeeva, L. and Y.I. Aristov, *Composites 'salt inside porous matrix'for adsorption heat transformation: a current state-of-the-art and new trends.* International Journal of Low-Carbon Technologies, 2012. **7**(4): p. 288-302. https://doi.org/10.1093/ijlct/cts050.
[46] Korhammer, K., et al., *Sorption and thermal characterization of composite materials based on chlorides for thermal energy storage*. Applied Energy, 2016. **162**: p. 1462-1472. https://doi.org/10.1016/j.apenergy.2015.08.037.
[47] Dawoud, B. and Y. Aristov, *Experimental study on the kinetics of water vapor sorption on selective water sorbents, silica gel and alumina under typical operating conditions of sorption heat pumps.* International Journal of Heat and Mass Transfer, 2003. **46**(2): p. 273-281. https://doi.org/10.1016/S0017-9310(02)00288-0.
[48] Tokarev, M., et al., *New composite sorbent CaCl2 in mesopores for sorption cooling/heating*. International Journal of Thermal Sciences, 2002. **41**(5): p. 470-474. https://doi.org/10.1016/S1290-0729(02)01339-X.
[49] Sharma, S.D., H. Kitano, and K. Sagara, *Phase change materials for low temperature solar thermal applications.* Res. Rep. Fac. Eng. Mie Univ, 2004. **29**(1): p. 31-64.
[50] Kaygusuz, K., *Experimental and theoretical investigation of latent heat storage for water based solar heating systems*. Energy conversion and management, 1995. **36**(5): p. 315-323. https://doi.org/10.1016/0196-8904(95)98896-U.
[51] Wang, R. and R.G. Oliveira, *Adsorption refrigeration—an efficient way to make good use of waste heat and solar energy*. Progress in energy and combustion science, 2006. **32**(4): p. 424-458. https://doi.org/10.1016/j.pecs.2006.01.002.
[52] Gibson, L.J. and M.F. Ashby, *The mechanics of foams: basic results*, in *Cellular Solids: Structure and Properties*, L.J. Gibson and M.F. Ashby, Editors. 1997, Cambridge University Press: Cambridge. p. 175-234.
[53] Giani, L., et al., *Washcoating method for Pd/γ-Al2O3 deposition on metallic foams.* Applied Catalysis B: Environmental, 2006. **62**(1-2): p. 121-131. https://doi.org/10.1016/j.apcatb.2005.07.003.
[54] Khouri, S., et al., *Metallurgical brownfields re-use in the conditions of Slovakia–A case study*. Metalurgija, 2016. **55**(3): p. 500-502. https://hrcak.srce.hr/153695.
[55] Gallagher, P.K., *Chapter 4 - Thermogravimetry and Thermomagnetometry*, in *Handbook of Thermal Analysis and Calorimetry*, M.E. Brown, Editor. 1998, Elsevier Science B.V. p. 225-278.
[56] Greenspan, L., *Humidity fixed points of binary saturated aqueous solutions.* Journal of research of the National Bureau of Standards. Section A, Physics and chemistry, 1977. **81**(1): p. 89. https://doi.org/10.6028/jres.081A.011.

[57] Danilatos, G., *Introduction to the ESEM instrument.* Microscopy research and technique, 1993. **25**(5-6): p. 354-361. https://doi.org/10.1002/jemt.1070250503.
[58] Donald, A.M., *The use of environmental scanning electron microscopy for imaging wet and insulating materials.* Nature materials, 2003. **2**(8): p. 511-516. https://doi.org/10.1038/nmat898.
[59] Ushak, S., et al., *Characterization of calcium chloride tetrahydrate as a phase change material and thermodynamic analysis of the results.* Renewable Energy, 2016. **95**: p. 213-224. https://doi.org/10.1016/j.renene.2016.04.012.
[60] Meisingset, K.K. and F. Grønvold, *Thermodynamic properties and phase transitions of salt hydrates between 270 and 400 K IV. CaCl2· 6H2O, CaCl2· 4H2O, CaCl2· 2H2O, and FeCl3· 6H2O.* The Journal of Chemical Thermodynamics, 1986. **18**(2): p. 159-173. https://doi.org/10.1016/0021-9614(86)90130-8.
[61] Cao, F. and B. Yang, *Supercooling suppression of microencapsulated phase change materials by optimizing shell composition and structure.* Applied Energy, 2014. **113**: p. 1512-1518. https://doi.org/10.1016/j.apenergy.2013.08.048.
[62] Faucheux, M., et al., *Influence of surface roughness on the supercooling degree: Case of selected water/ethanol solutions frozen on aluminium surfaces.* International journal of refrigeration, 2006. **29**(7): p. 1218-1224. https://doi.org/10.1016/j.ijrefrig.2006.01.002.
[63] Safari, A., et al., *A review on supercooling of Phase Change Materials in thermal energy storage systems.* Renewable and Sustainable Energy Reviews, 2017. **70**: p. 905-919. https://doi.org/10.1016/j.rser.2016.11.272.
[64] Mohapatra, D. and J. Nandanavanam, *Salt in matrix for thermochemical energy storage-A review.* Materials Today: Proceedings, 2022. https://doi.org/10.1016/j.matpr.2022.05.453.
[65] Xiao, X., P. Zhang, and M. Li, *Effective thermal conductivity of open-cell metal foams impregnated with pure paraffin for latent heat storage.* International Journal of Thermal Sciences, 2014. **81**: p. 94-105. https://doi.org/10.1016/j.ijthermalsci.2014.03.006.
[66] N'Tsoukpoe, K.E., et al., *A review on the use of calcium chloride in applied thermal engineering.* Applied Thermal Engineering, 2015. **75**: p. 513-531. https://doi.org/10.1016/j.applthermaleng.2014.09.047.
[67] Ren, S., et al., *Corrosion testing of metals in contact with calcium chloride hexahydrate used for thermal energy storage.* Materials and Corrosion, 2017. **68**(10): p. 1046-1056. https://doi.org/10.1002/maco.201709432.
[68] Peng, C., L. Chen, and M. Tang, *A database for deliquescence and efflorescence relative humidities of compounds with atmospheric relevance.* Fundamental Research, 2021. https://doi.org/10.1016/j.fmre.2021.11.021.
[69] Kelly, J.T. and A.S. Wexler, *Thermodynamics of carbonates and hydrates related to heterogeneous reactions involving mineral aerosol.* Journal of Geophysical Research: Atmospheres, 2005. **110**(D11). https://doi.org/10.1029/2004JD005583.
[70] Council, N.R., *International Critical Tables of Numerical Data, Physics, Chemistry and Technology*. 1930, Washington, DC: The National Academies Press.

Highlights

- Composite material based on metal foam and $CaCl_2$ for thermochemical heat storage is developed.
- Cyclic stability and heat released during hydration are significantly enhanced.
- Evolution of thermochemical performance and improvement mechanism are revealed.
- Offering both mechanical and thermochemical benefits for thermal energy storage.

Cover letter

Dear Editorial Board,

We wish to submit the enclosed manuscript entitled "Newly designed metal foam-salt hydrate composite for thermochemical energy storage" for consideration by *Applied Energy*. We confirm that this work is original and has not been published elsewhere, nor is it currently under consideration for publication elsewhere, in whole or in part. We wish to publish this manuscript for the following reasons:

Thermochemical heat storage systems based on the sorption mechanism between water vapor and hygroscopic salts are considered to be a promising technology. However, hygroscopic salts have drawbacks such as swelling and agglomeration of the crystalline salt particles during hydration/dehydration cycles, which progressively leads to decreasing specific reaction surface and kinetics of heat and mass transfer, thus resulting in poor cyclic performance and stability. A family of composite sorbents named Selective Water Sorbents (SWS) have been studied to alleviate the limitations mentioned above, with hygroscopic salts and host matrices with nanoscale pore size (< 50 nm). Despite the high energy density, problems related to inappropriate charging temperature, low thermal conductivity and possible leakage of the salt solution after deliquescence have impeded its large-scale applications.

The novelty of our work is the development of an original SWS composite, based on open-cell metal foam with pore size of 350 μm as host matrix, containing calcium chloride as hygroscopic salt dispersed in the pores. An open-cell metal foam host matrix improves the heat and mass transfer kinetics thanks to the porous structure and the high thermal conductivity, and offers additional advantages related to elevated mechanical strength, which would ensure mechanical resistance of the composite.

The experimental results showed that the composite presented significant improvement in thermochemical performance compared to that of bulk calcium chloride powder in hydration/dehydration cycles. For cyclic stability, composites presented a slight increase and stabilization of thermal energy released upon cycles, while salt showed a substantial and continuous degradation of 78.5% in performance after 12 cycles. For heat released, composites outperformed considerably the bulk calcium chloride in almost all cycles. At the 12^{th} cycle, the heat released of composites improved substantially to 5~6 times that of bulk calcium chloride powder. Observations by in situ environmental scanning electron microscope (ESEM) hydration/dehydration cycles demonstrated that swelling and deliquescence induce moderate redistribution of salt hydrates within the metal foam while preserving the essential open porosity of the matrix. It efficiently prevents extensive salt agglomeration and loss of specific reaction area, which explains the amelioration of the composite's thermochemical properties and their cyclic stability.

In conclusion, the metal foam-salt hydrate composite developed in our work is suitable and promising for thermochemical energy storage, offering both mechanical and thermochemical advantages.

This work opens up innovative possibilities for research in sorption thermochemical energy storage systems. That's way we believe that this manuscript fits the aims and scope of *Applied Energy*. Therefore, if we could have the honor of publishing this work in *Applied Energy*, we would greatly appreciate the opportunity to share and discuss this research with all other readers of this journal.

To answer other questions indicated in the Guide for authors, 1) the paper is more appealing to a scientific audience. 2) I'm available as a reviewer for at least three other articles for *Applied Energy* during the current year.

If you require any additional information regarding our manuscript, please do not hesitate to contact me via the resources below. We greatly appreciate your time and consideration.

Sincerely,

Yutong Liu
Ecole Polytechnique
yutong.liu@polytechnique.edu.